LASER INTERFEROMETER GRAVITATIONAL WAVE OBSERVATORY
- LIGO -
CALIFORNIA INSTITUTE OF TECHNOLOGY
MASSACHUSETTS INSTITUTE OF TECHNOLOGY

Technical Note	**LIGO-T22xxxxx–**	2026/09/25

Optical Enhancement Cavity Project Final Report

Jack Ryan, Rana Adhikari, Georgia Bolingbroke

California Institute of Technology
LIGO Project, MC100-36
Pasadena, CA 91125
Phone (626) 395-2129
Fax (626) 304-9834
E-mail: info@ligo.caltech.edu

Massachusetts Institute of Technology
LIGO Project, Room NW22-295
Cambridge, MA 02139
Phone (617) 253-4824
Fax (617) 253-7014
E-mail: info@ligo.mit.edu

LIGO Hanford Observatory
Route 10, Mile Marker 2
Richland, WA 99352
Phone (509) 372-8106
Fax (509) 372-8137
E-mail: info@ligo.caltech.edu

LIGO Livingston Observatory
19100 LIGO Lane
Livingston, LA 70754
Phone (225) 686-3100
Fax (225) 686-7189
E-mail: info@ligo.caltech.edu

http://www.ligo.caltech.edu/

Abstract

Blue Laser Fusion (BLF) is working to establish the world's first commercial inertial fusion energy (IFE), building on the National Ignition Facility's breakthrough demonstrating a fusion target gain in 2022 [1]. BLF utilizes Coherent Beam Combining (CBC) technology and an Optical Enhancement Cavity (OEC) to produce a highly efficient high energy pulsed laser system suitable for laser fusion. Because fusion ignition requires extremely high energy densities, laser fusion systems must operate in a pulsed regime to maximize peak power on the target. In prior work with the Adhikari group at Caltech, a 1.5m prototype cavity operating in the continuous wave (CW) regime achieved an optical enhancement of 58,461 yielding kilowatt-level circulating powers. This project extends that work towards pulsed operation of the laser. The primary objective of this project is to demonstrate pulse-locking of the laser to the OEC, characterize the pulse bandwidth and temporal shape, and understand the technical challenges involved in maintaining a pulse lock. Work to date has focused on reestablishing the past working setup within an improved vacuum system. This included reinstalling 3.4 ppm loss mirrors within the vacuum chamber to reestablish the OEC, profiling and aligning the beam to the cavity axis, and achieving a cavity lock under CW operation utilizing the Pound-Drever-Hall laser locking technique. This project has resulted in significant progress towards establishing a demonstration cavity setup capable of examining pulse-dynamics. Challenges associated with low optical coupling efficiency to the OEC were also explored, with several potential solutions to these challenges being identified and investigated.

Contents

1 Introduction **3**

2 Background **3**

3 Project Objectives **6**

4 Methods **7**

4.1 Beam Profiling 7

4.2 Mode Matching 7

4.3 Aligning the Cavity 9

4.4 PDH Lock 9

4.5 Error Signal Analysis 11

4.6 Lock Analysis 12

4.7 Cavity Ring Down Measurement 16

4.8 Challenges 18

5 Future Steps **20**

5.1 Pulse Locking 20

5.2 Pulse Characterization 20

5.3 Dither Lock 20

6 Conclusion **22**

7 Acknowledgements **23**

1 Introduction

The Laser Interferometer Gravitational-wave Observatory (LIGO), utilizes long baseline Michelson interferometers to detect gravitational waves (GWs) generated by astronomical events such as black hole mergers or neutron star collisions. As GWs pass through each detector, they warp space-time, changing the path-length difference of the Michelson interferometers leading to a detectable signal. LIGO increases detector sensitivity through the use of Fabry-Perot cavities within each Michelson arm. The cavities provide power build up, which enhances the modulation GWs cause, increasing detector sensitivity.

This principle of utilizing optical cavities to build up high amounts of optical power has broad applications across physics, including in laser inertial confinement fusion.

Blue Laser Fusion (BLF) is working to establish the world's first comercial inertial fusion energy (IFE) generation building upon the National Ignition Facility's demonstration of fusion target gain in 2022 [1]. BLF utilizes Coherent Beam Combination (CBC) technology and an Optical Enhancement Cavity (OEC) to produce a highly efficient pulsed laser system capable of producing 10 kJ pulses at repetition rates of 1 to 10 Hz. Through the combination of 500 of these systems, BLF aims to generate 5 MJ pulses at high repetition rates for fusion ignition [3].

The focus of this project was on devoloping and understanding the OEC dynamics and technical limitations. The BLF OEC is a Fabry-Perot optical cavity capable of building up and storing high intracavity powers. Prior work on the Caltech OEC has achieved enhancement of a continuous wave (CW) laser by a factor of 58,461, achieving circulating powers of several kW within a 1.5 m demonstration cavity [4]. A key next step for the OEC is to operate the OEC in the pulsed regime. Pulsed operation of the OEC obtains the high peak powers required for inertial fusion, but introduces significant challenges.

This project worked to establish the past OEC setup within a new vacuum system. Key results included profiling and mode matching the beam to the cavity eigenmode. Obtaining a stable CW lock through the PDH locking procedure, and exploring solutions to a lack of power coupled into the cavity. Future work will explore the pulse dynamics of the laser within the now reestablished OEC system, and work done can be adopted to the 15 m and 150 m OEC cavities under development at BLF.

2 Background

The OEC is a standard Fabry-Perot optical cavity consisting of two highly reflective mirrors. Light directed into the cavity that satisfies the resonant condition

$$n\lambda = 2L \tag{1}$$

where λ is the wavelength of incident light, L is the length of the cavity, and n is an integer, builds up over time. This is because accumulated phase of circulating light matches the phase of new incident light, constructively interfering.

Related to this resonance condition is the free spectral range (FSR) of the cavity, which is

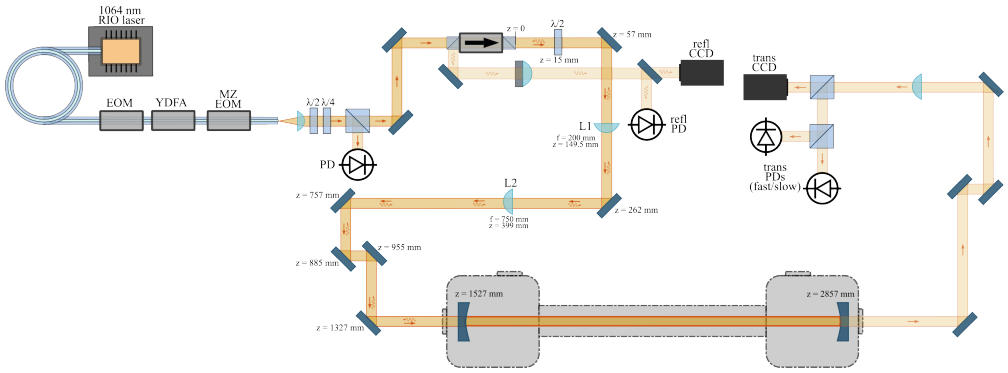


Figure 1: Schematic of current OEC setup. Figure credit: Georgia Bolingbroke

a measure of the frequency spacing between resonant peaks. By substituting $c/f = \lambda$ into Eq. 1, we see that the distance between resonant peaks is given by

$$FSR = \frac{nc}{2L} \tag{2}$$

with resonant peaks contained at an integer multiple of the FSR.

A measure of how well light is stored in the cavity is called the finesse, measuring the average number of times a photon circulates before it exits the cavity. The theoretical finesse of the optical cavity is given by

$$Finesse \approx \frac{\pi(R_1R_2)^{1/4}}{1-(R_1R_2)^{1/2}} \tag{3}$$

where R is the reflectivity of the mirrors. The OEC is a cavity with ultra-high finesse, with each mirror having a loss of only 3.4 parts-per-million (ppm). Assuming no additional losses in the cavity, the mirror transmission values yield a theoretical finesse of approximately 924,000. In practice, the finesse will be lower than this value as intracavity losses occur due to stray dust and imperfect alignment, non uniform mirror coatings, and imperfect cleaning.

To minimize these losses, the OEC is contained within an ultra-high-vacuum (UHV) chamber capable of reaching pressures of 10^{-7} torr. Prior to this project, significant work with the OEC has already been completed as summarized in Ref. [4]. Through this work, the OEC achieved a finesse of 419,000.

The FSR and finesse of the cavity are related through

$$Finesse = \frac{FSR}{\Delta\nu} \tag{4}$$

where $\Delta\nu$ is the linewidth of the cavity's resonant condition. Using the estimated finesse and FSR of the OEC, the linewidth of the cavity is approximately 250 Hz. This extremely narrow linewidth, along with seismic noise, laser drifting, and thermal fluctuations necessitates the usage of feedback to keep the laser locked to the cavity resonance, which will be covered in depth in the methods section.

Mode matching is also critical for operation of the OEC. When coupling the input laser beam, which has a Gaussian profile, into the OEC, only a certain set of transverse electromagnetic (TEM) modes, are allowed by boundary conditions [5]. To efficiently couple power into the cavity, we want to match the incoming beam shape to the fundamental TEM_{00} mode of the cavity, avoiding excess power into higher order modes (HOMs).

To mode match, the beam's Gaussian shape described by the q-parameter

$$q(z) = z - z_0 + iz_R, \qquad z_R = \frac{\pi w_0^2}{\lambda}, \tag{5}$$

where w_0 is the beam waist, z the distance, z_R the Rayleigh range, and λ the wavelength, is shaped utilizing lenses to spatially match the cavity's TEM_{00} eigenmode at the input mirror. To find the shape of the TEM_{00} eigenmode, ABCD matrices are utilized.

Within an optical system, the propagation of a Gaussian beam can be described by ABCD matrices, with optical components such as mirrors, beam splitters, and lenses having unique transfer matrices, covered in Ref. [5].

To find the TEM_{00} eigenmode of the optical cavity, we require that the mode must reproduce itself after each round trip. This gives the condition

$$q_{cav} = q_1 = \frac{Aq_1 + B}{Cq_1 + D}. \tag{6}$$

Which can be rearranged to give the following quadratic equation

$$Cq_{cav}^2 + (D - A)q_{cav} - B = 0 \tag{7}$$

By solving this equation, we can solve for q_{cav}, and find the eigenmode's waist size, location, and spot size at the input mirror. Once these parameters are known, a mode matching solution utilizing two to three lenses is found to match the beam's q-parameter to q_{cav} as closely as possible, maximizing the circulating power into the cavity [5].

The geometric stability of a Fabry-Perot optical cavity is also important to consider. This can be given by the mirror g-factors, given by $g_i = 1 - L/R_i$, where R_i is the radius of curvature of each mirror. A cavity is stable when

$$0 \leq g_1 g_2 \leq 1 \tag{8}$$

For the OEC, with $L = 1.33$ m and $R_1 = R_2 = 15$ m, each mirror has $g = 0.911$, giving $g_1 g_2 = 0.831$. This places the cavity within the stable region, with some tolerance to thermal effects affecting the radius of curvature of each mirror.

A summary of relevant cavity parameters for OEC are given below. Note, the new vacuum system has shortened the length of the cavity from 1.5 m to 1.33 m. This has led to a corresponding increase in the theoretical FSR.

Table 1: Optical enhancement cavity parameters.

Parameter	Value
Cavity length, L	1.33 m
Free spectral range, $c/2L$	112.7 MHz
Finesse, $\mathcal{F}$	419,000
Mirror transmissivity, T	3.4 ppm
Mirror radius of curvature, R_c	15 m
g factor	0.831

3 Project Objectives

Prior work with the OEC has achieved stable locking to an ultra-high-finesse cavity with the laser operating as a continous wave (CW), however, additional challenges arise when attempting to lock the cavity with a pulsed laser [4]. This is because a coherent build up of optical pulses requires the FSR to precisely match the pulse rate of the laser. Addressing and overcoming these challenges is an integral part of this project, and the techniques developed and learned will be utilized within BLF's larger 15 m and 150 m cavities. To achieve the larger objective of pulse locking, this project seeks to achieve several smaller goals outlined below:

Integrate mirrors and realign cavity within new vacuum system

Past work on the OEC was conducted with a different vacuum system, which has since been improved. A first objective of this project is to reestablish the previous working setup. This includes implementing a set of 3.4 ppm loss mirrors into the OEC, recalculating the new cavity's eigenmode, mode matching to this eigenmode and aligning the beam to cavity the cavity axis.

Achieve a stable continous wave lock to the OEC

Once a working setup of the OEC has been achieved, we will lock the cavity to the TEM_{00} mode. This will require the use of a Pound-Drever-Hall (PDH) lock, covered in depth in the Methods section.

Characterize pulse shape

Once the cavity has been aligned and locked, we will characterize the pulsed laser. This will include understanding the temporal pulse shape, bandwidth, and electronics involved in generating and observing the pulses.

Perform pulse locking on OEC

Once the pulses have been characterized, we will lock the pulsed laser to the OEC by a dither lock. This is done by varying the repetition rate of the laser pulses. If time permits, we will also investigate an improved form of locking through balanced homodyne readout.

Analyze results and address limitations

Since the OEC is a demonstration cavity, a key objective is to understand and interpret the procedure, limitations, and effectiveness of pulse locking to the cavity. The techniques we

use and develop can then be adapted to the larger BLF cavities in development.

4 Methods

During the first week of this project, I gained familiarity with the cavity setup through simulations using the Finesse Python package. I modeled the OEC and the expected error signal derived for the PDH lock, as well as the generation of higher order modes from cavity misalignment. Additionally, I reviewed literature on cavity mode matching and ABDC formulation for optics.

During the second week the new set of cavity mirrors with 3.4 ppm loss and radius of curvature of 15 m were installed. To align the cavity, we first installed the output cavity mirror, and aligned the mirror until the reflected beam overlapped with the incident beam path. Then, we installed the input mirror, and once again adjust the alignment until the input beam overlapped with the reflected beam. Fine adjustments were completed with the input steering mirrors until the beams were completely overlapped. The aligned beam path was marked with a set of 5 irises for future realignment.

4.1 Beam Profiling

As the cavity location and length had changed from the prior setup, a new mode matching solution was required. To find this solution, the first step was to find the profile of the beam to obtain the waist location and waist quadrature measurements necessary for new mode matching solution.

To profile the beam, a WinCamD beam profiler was set in the beam path after the Faraday isolator (FI), where z=0 denotes the edge of the FI shown in Fig. 1. DataRay software was utilized to take 5 waist measurements every 5 mm in reference to a ruler. The waist versus distance data was then imported into Python and fit to the waist equation given by

$$w(z) = w_0\sqrt{1 + (\frac{z}{z_R})^2} \tag{9}$$

where w(z) is the waist as a function of distance, z, and z_R is the Rayleigh range. The fit versus distance along with the residuals is shown below in Fig. 2.

4.2 Mode Matching

After profiling the beam, the waist, waist position (z0), and Rayleigh range found from the fit were utilized to compute a new mode matching solution for the cavity following the ABCD matrix formulation discussed in the background section.

The solution found consisted of two lens shown in Fig. 1, with locations and focal lengths given in Table 2 for reference. After implementing the lenses, the beam was realigned to the cavity axis by steering through all 5 irises.

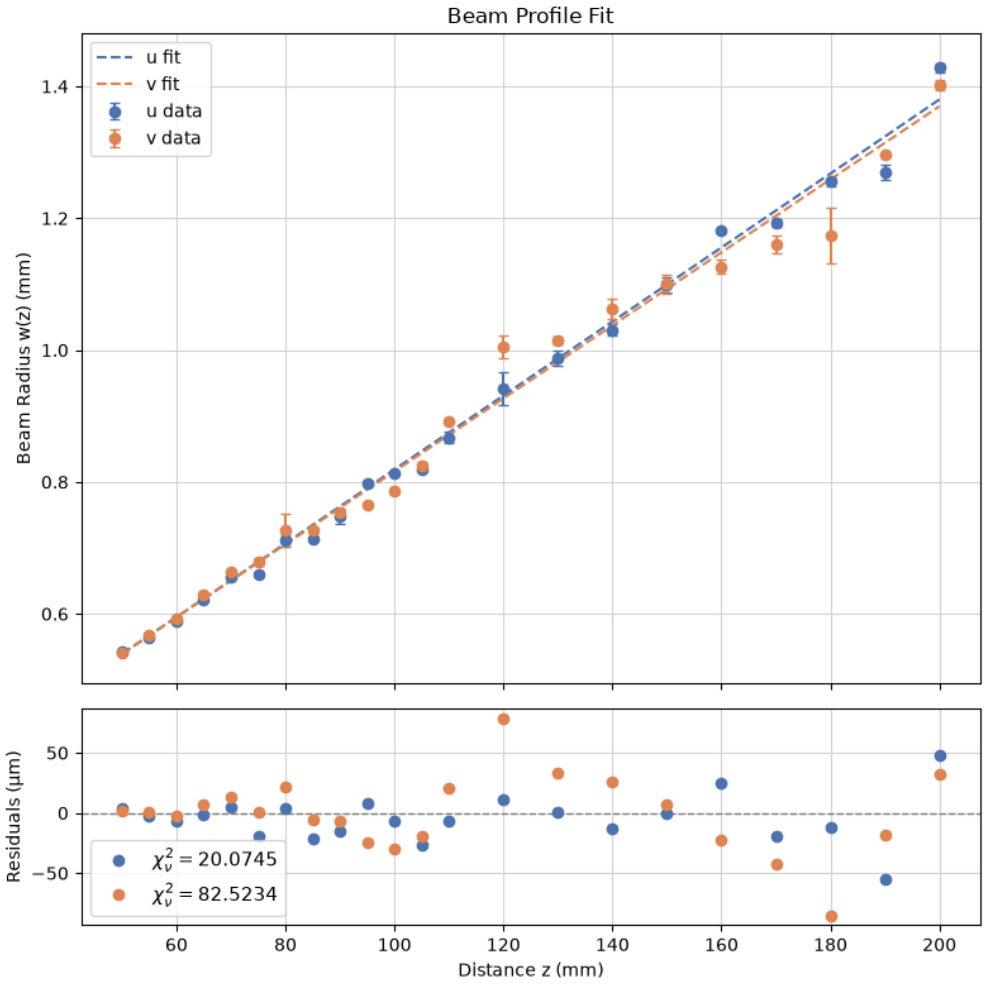


Figure 2: Gaussian beam fit (top) and residuals of fit (bottom).

Table 2: Mode-matching lens positions, measured from the Faraday isolator (FI).

Lens	Position after FI (mm)	Focal length (mm)
Lens 1	149.5	200
Lens 2	399.4	750

This procedure of profiling and mode matching was done several times throughout the summer. This was done a change in the fiber output coupler partway through the summer, which changed the profile of the beam as it went to freespace. Later in the summer, we also reprofiled the beam due to low transmitted power on resonance, which we believed was due to poor mode matching. This process will be further covered below in the challenges section of the report.

4.3 Aligning the Cavity

With the beam coarsely aligned through the irises to the cavity, the transmitted CCD camera was used to visualize the cavity modes. An aligned cavity will show a strong TEM_{00} mode, with no coresonant HOMs present. HOMs were present prior to input steering alignment, which provide guidance of which way to adjust the steering. A HOM with modes that expand horizontally indicate the input beam is misaligned in yaw while a HOM that expands vertically indicates misalignment in pitch. Finally, ring shaped modes indicate poor mode matching. The pitch and yaw of the beam was finely adjusted with the input steering mirrors while the lens locations were finely tuned with a linear stage until a strong TEM_{00} peak was observed. Figure 3 showcases an example of the observed HOM and TEM_{00} mode.

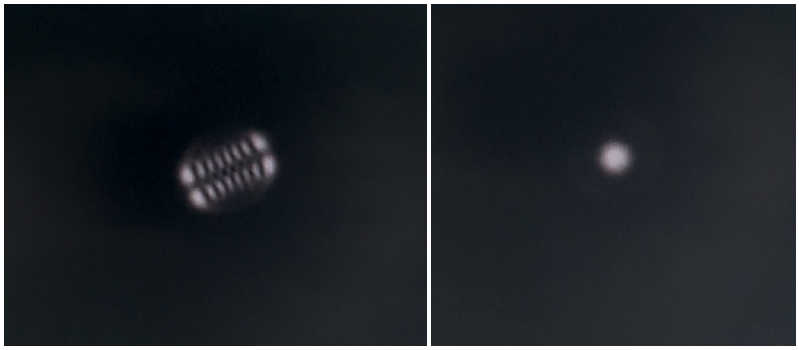


Figure 3: HOM (left), misaligned in pitch and yaw, and TEM_{00} (right).

4.4 PDH Lock

After aligning the cavity, the next step was to achieve a stable lock of the OEC through the PDH covered in depth by Black in Ref. [6]. The PDH method allows for the power observed at the reflection photodetector, which is symmetric about resonance and thus provides no indication on which way to tune the laser, to be converted into an error signal which is antisymmetric about resonance, allowing for tuning of the laser frequency towards cavity resonance.

The first step to performing a PDH lock to the OEC was to use a fiber coupled Electro-Optic Modulator (EOM) to generate frequency sidebands of the laser at 20 MHz. Following Black's notation, phase modulation of the beam at frequency Ω produces a carrier and two sidebands above and below the carrier frequency [6], given by

$$E_{\text{inc}} \approx E_0 \left[J_0(\beta)\, e^{i\omega t} + J_1(\beta)\, e^{i(\omega+\Omega)t} - J_1(\beta)\, e^{i(\omega-\Omega)t} \right] \tag{10}$$

where β is the modulation depth and J_n are Bessel functions. The carrier power is $P_c = J_0^2(\beta)P_0$ and the power in each first-order sideband is $P_s = J_1^2(\beta)P_0$, with P_0 the total incident power.

This modulated light was then directed into the OEC, where the sidebands are off resonance and promptly reflect at the input mirror, while the carrier light enters the cavity depending on beam mode matching, alignment and impedance matching. Light that enters into the cavity will acquire a phase shift before it leaks out. Each frequency component is reflected according to the cavity's reflection coefficient, given by

$$F(\omega) = \frac{E_{\text{refl}}}{E_{\text{inc}}} = \frac{r\left(\exp\left(i\dfrac{\omega}{\Delta\nu_{\text{fsr}}}\right) - 1\right)}{1 - r^2 \exp\left(i\dfrac{\omega}{\Delta\nu_{\text{fsr}}}\right)} \tag{11}$$

where r is the amplitude reflection coefficient of the cavity mirrors and $\Delta\nu_{\text{fsr}}$ the free spectral range. The combination of the carrier's leakage light and the promptly reflected sidebands is then directed onto the reflection PD.

The power incident on the reflection PD is the sum of the reflected carrier and the sidebands, given by

$$\begin{aligned} P_{\text{refl}} = {} & P_c|F(\omega)|^2 + P_s\left\{|F(\omega+\Omega)|^2 + |F(\omega-\Omega)|^2\right\} \\ & + 2\sqrt{P_c P_s}\Big\{ \text{Re}\left[F(\omega)F^*(\omega+\Omega) - F^*(\omega)F(\omega-\Omega)\right]\cos(\Omega t) \\ & \quad + \text{Im}\left[F(\omega)F^*(\omega+\Omega) - F^*(\omega)F(\omega-\Omega)\right]\sin(\Omega t)\Big\} + (2\Omega \text{ terms}) \end{aligned} \tag{12}$$

Within this expression, we are interested in the terms multiplied by the $\cos(\Omega t)$ and $\sin(\Omega t)$, as they contain information relevant to the carrier fields accumulated phase in the cavity.

From here, to extract the error signal, the signal measured at the reflection PD was then given to our Moku, where it was mixed at the EOM frequency of 20 MHz. This is due to the simple trig identity given by

$$\sin(\Omega t)\sin(\Omega' t) = \frac{1}{2}\left\{\cos\left[(\Omega-\Omega')t\right] - \cos\left[(\Omega+\Omega')t\right]\right\} \tag{13}$$

where we see that multiplying two sine functions yields two cosine terms. When the mixing signal frequency equals the EOM modulation frequency, one of the cosine terms becomes a

DC term. A similar trig identity holds for mixing of the cosine term in Eq. 12. A phase offset was also utilized during this step to isolate either the cosine or sine term.

To extract this DC signal, the mixed signal was passed through a low pass filter set to 10 MHz within the Moku. Finally, this isolates the term in Eq. 12 oscillating at Ω, giving the PDH error signal

$$\varepsilon = -2\sqrt{P_c P_s}\ \mathrm{Im}\left\{F(\omega)F^*(\omega+\Omega) - F^*(\omega)F(\omega-\Omega)\right\} \tag{14}$$

4.5 Error Signal Analysis

After making improvements to the alignment of the cavity, we were able to observe an error signal. The error signal was created utilizing the following setup: We modulated our fiber-coupled EOM at 20 MHz with a modulation depth of $\beta = 0.3$ (95 % of power in the central carrier) utilizing a MokuPro. The generated sidebands followed the reflection path denoted in Fig. 1 and, where they were incident onto a New Focus 1611 PD, which was AC coupled, had a bandwidth of 1 GHz, and transimpedance gain of 700 V/A.

Figure 4 below showcases a steady-state simulation of the expected error signal derived from the same loop settings utilized for the lock. The important feature to note is the amplitude of the error signal, which is approximately 400 mV.

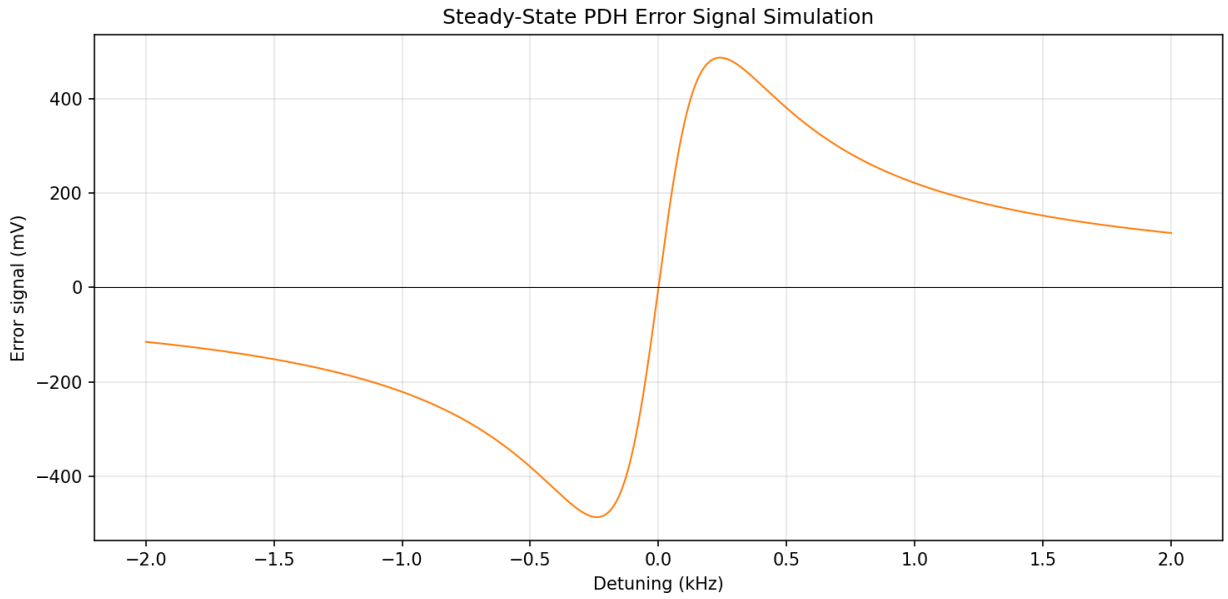


Figure 4: Steady-State PDH error signal simulation for OEC of 400,000 finesse, 20 ppm intracavity losses, and 3.4 ppm transmisivity mirrors.

Figure 5 showcases the actual error signal observed from the OEC. It is immediately clear that the steady-state approximation does not account for the time dependency of the signal due to transients. Transients occur because of the cavity's extremely narrow linewidth, and relatively long buildup time. Because of this, laser, seismic, and accoustic noise all contribute

to a ring-down effect, where the laser frequency rapidly sweeps through resonance without building up to the steady-state field. When this occurs, light will leak out of the cavity, and interfere with incident light, resulting in the exponentially decaying interference signal.

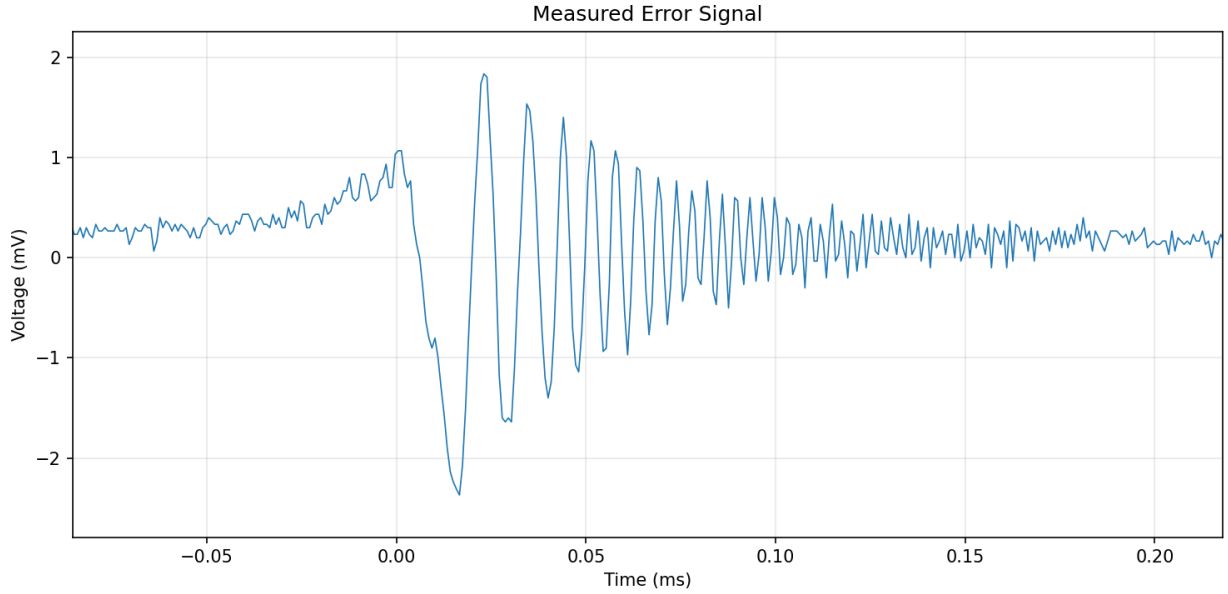


Figure 5: Observed error signal measured with MokuPro. Note the observed exponential ring down behavior of the signal, and the amplitude of approximately 2 mV.

Comparing the simulation to the observed signal, it is immediately clear that the observed signal is approximately 0.5% of the expected signal amplitude. This discrepancy led to significant challenges in aquiring a lock for the first time, and its potential causes will be discussed in more depth below in the challenges section.

Finally, Figure 6 is a simulation of the expected error signal derived form our PDH setup considering the observed transient behaviour. We can see that modeling the laser frequency as rapidly changing on the order of tens of MHz per second recovers the observed ring down effect. As was previously stated, this change of frequency is a likely combination of a number of factors, like seismic noise shaking mirror mounts, laser frequency noise, and thermal fluctuations in the system. It is important to note that despite the transient behavior and small amplitude of the error signal, we were able to obtain and keep a stable lock to the OEC consistently with lengths greater than 10 minutes.

4.6 Lock Analysis

We continously optimized the PID loop settings throughout the summer to improve the stability of the lock. At first, this was done qualitatively by making fine adjustments to the gain of each parameter until the lock time lengthened. After achieving a lock of several minutes, however, we analyzed the open loop transfer function and noise budget of the lock to inform our future adjustments.

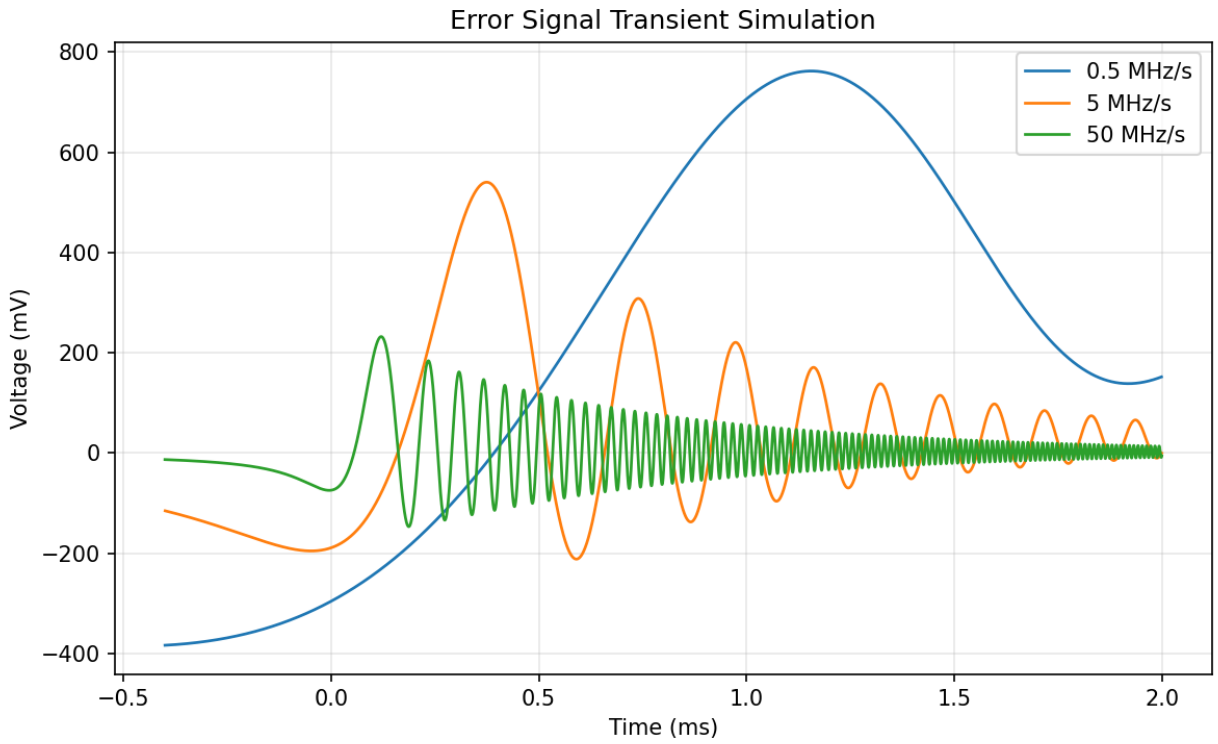


Figure 6: Transient simulation. A modeled sweep of greater than 50 MHz/s recovers the observed transient behavior.

To take the open loop transfer function (OLTF), a swept sine wave was mixed into the feedback signal generated from the PID loop before being fed into the laser. This process was done via Moku's internal Frequency Response Analyzer, where the swept sine was mixed with the feedback signal via the PID box, set to 0 dB of gain. The feedback signal was generated as usual, via Moku's Laser Lock Box. Results of this are shown below in Figure 7.

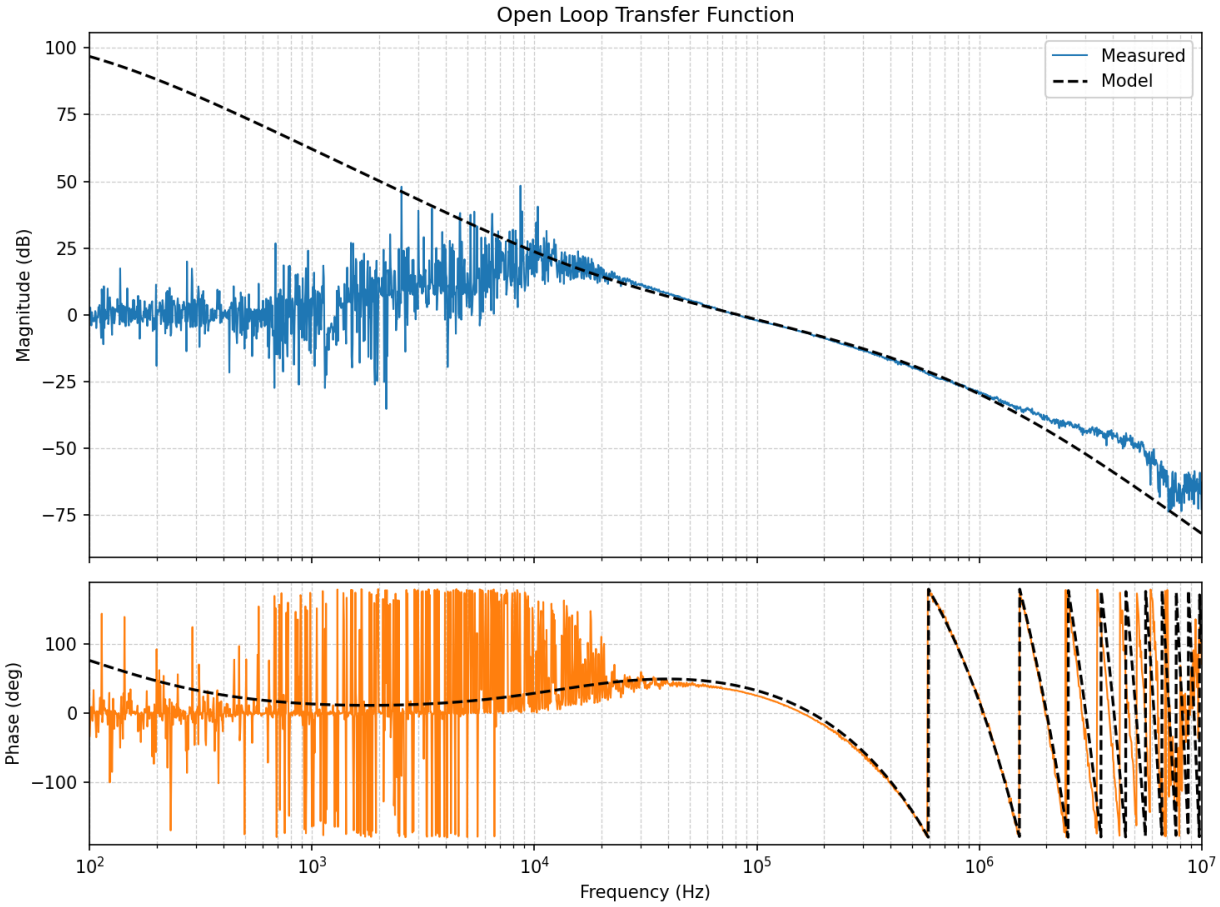


Figure 7: Open loop transfer function of OEC lock. Unity gain frequency is 80 kHz, corresponding to a phase margin of 30 degrees.

In Figure 7, a comparison to the modeled OLTF has also been provided. In the modeled OLTF, the same loop structure was incorporated, including the Moku's PID settings, with a integrator cutoff at 15 kHz, and differentiator cutoff at 85 kHz. When comparing to the model, we can see that at frequencies below 10 kHz, the measured OLTF significantly deviates. We believe this is due to the noise floor being above the swept sine amplitude. In the future, this can be improved with a new measurement with a stronger swept sine to better excite a response from the system above the noise floor.

An Amplitude Spectral Density (ASD) of both the error signal and the feedback signal generated by the PID loop was also taken to examine the lock's bandwidth and quality. The results are shown below in Fig 8.

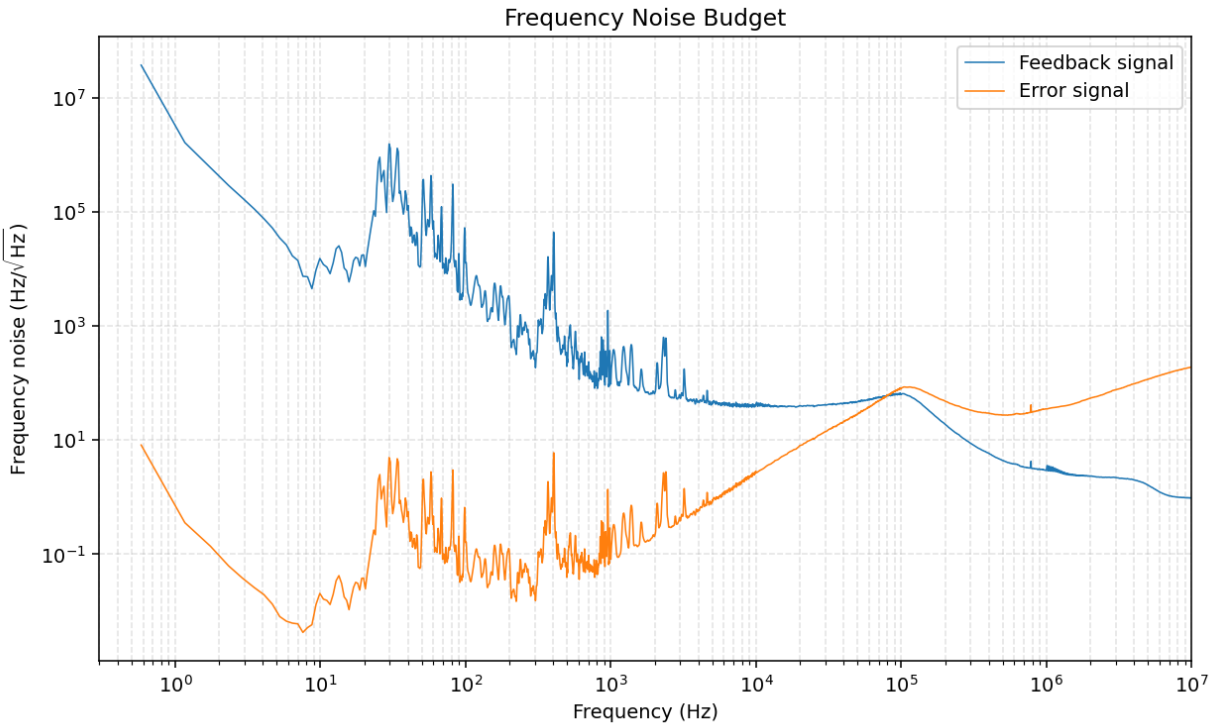


Figure 8: Noise budget of OEC lock. The PDH lock suppresses noise from the cavity to several orders of magnitude up to the unity gain frequency of 80 kHz.

From the OLTF and noise budget, we can see that our lock has a unity gain frequency, measuring the bandwidth at which the lock can provide feedback, at 80 KHz. With the OLTF, this corresponds to a phase margin of 30 degrees. From this, we can see that the differentiator within the PID loop is not providing feedback to the system, as its cutoff frequency was approximately 84 KHz, above the UGF. Going forward, the loop can be improved to utilize only a PI, which should also lower the noise at higher frequencies.

4.7 Cavity Ring Down Measurement

With the cavity locked, we proceeded with performing a cavity ring down (CRD) measurement to find the finesse of the OEC. In a CRD measurement, the laser beam is rapidly extinguished, allowing light that has built up in the cavity to slowly leak out in an exponential decay. This exponential decay follows

$$P(t) = P_o e^{-t/\tau} \tag{15}$$

With P_o the initial power, and $\tau = \frac{finesse*L}{\pi c}$. By fitting observed data to this exponential decay, the τ parameter can be determined giving a measure of the cavity finesse.

In our setup, to rapidly extinguish the beam we utilized a Mach-Zehnder (MZ) EOM. The max extinguishing ratio was found by stepping the minimum and maximum DC bias signal to minimize and maximize the measured power on the reflection PD. This maximum (4.05 V) and minimum (-0.40 V) bias was then input back into the MZ EOM as a square wave with a 0.1 Hz frequency and 20% duty cycle via a waveform generator. The cavity was then locked and the square wave output to the MZ EOM. Both the reflection PD and waveform generator outputs were sent to a 12 GHz oscilloscope, with a trigger set on the falling edge of the square wave to acquire the CRD waveform. The measured waveforms are shown below in Fig. 9.

Qualitatively, this appears how a CRD should look, with the power incident on the reflection PD exponentially decaying as the beam is rapidly extinguished. However, it was noticed that this same waveform was generated even when the cavity was not locked, when no intracavity field could build up. This points to the fact that we are not observing actual CRD, but rather the slow extinguishing of the beam by the MZ EOM.

To check this I setup a simple cavity ring down simulation utilizing python and the analytical reflected, intracavity, and transmitted fields given in Ref. [8], shown below in Fig. 10.

We can see that this shows that for our current cavity setup, with an estimated mode matching efficiency of 10%, it is better to perform the CRD measurement on the transmission PD, where the waveform is much clearer. Unfortunately, we were unable to align the fiber-coupled transmission PD as a result of very low transmission power. This meant that we were unable to recover enough beam power on the transmission side to align into the PD. While this setback faced during the project was significant and unfortunate, it also guided the last few weeks of the project. During these weeks, significant time was spent understanding potential sources for poor coupling into the cavity, as well as solutions. This process will be discussed below in the Challenges section.

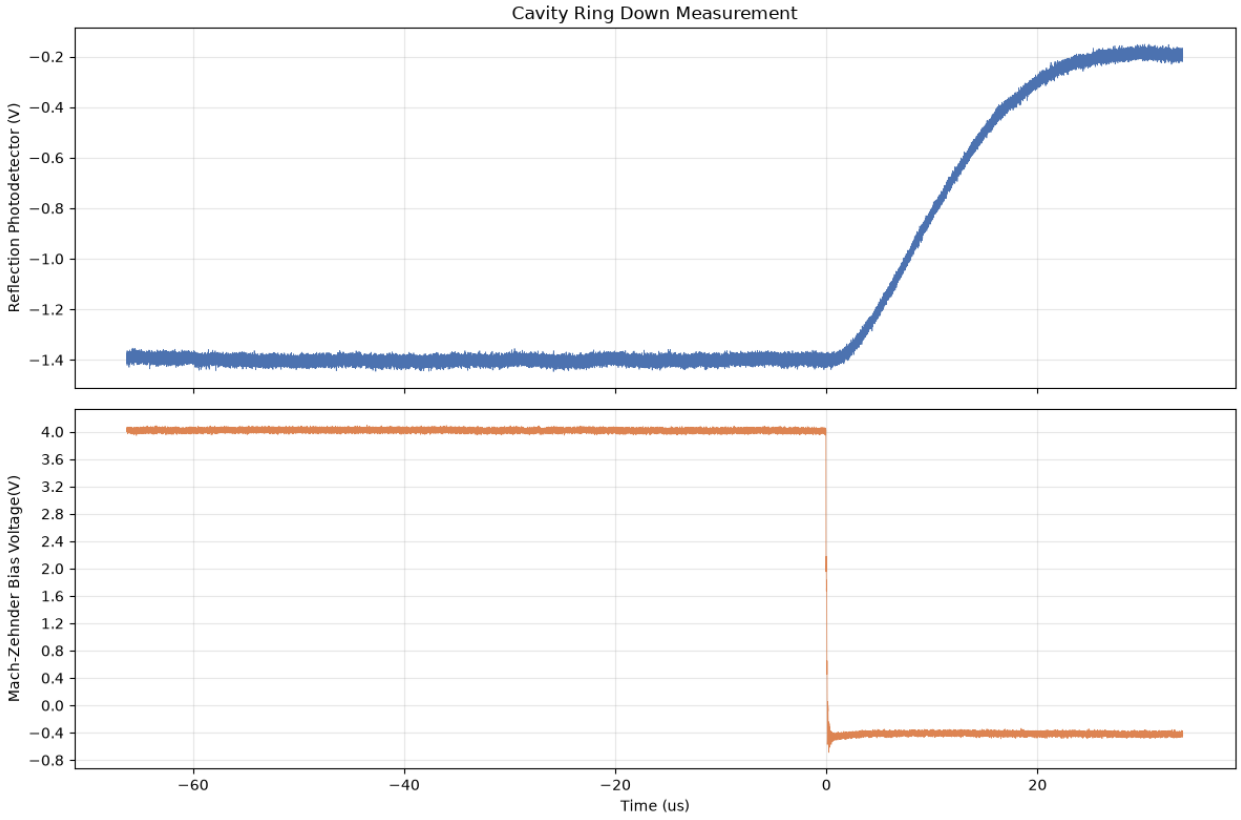


Figure 9: Cavity ring down results. Measured voltage on reflection PD (top) and MZ EOM input (bottom). Note, the reflection PD power is inverted due to the internal electronics of the PD.

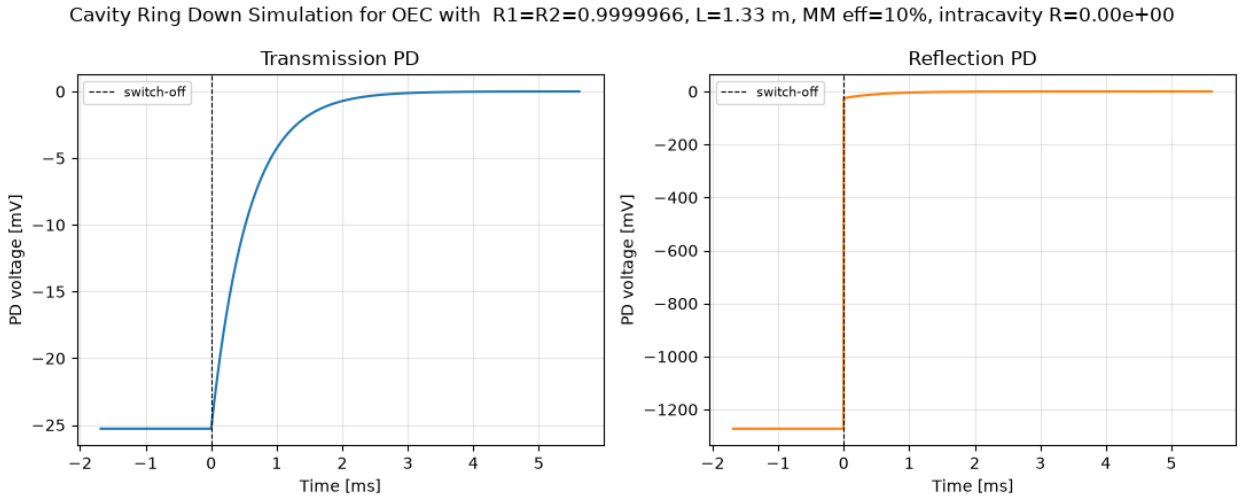


Figure 10: Simulation of expected cavity ring down curves on reflection and transmission photodetectors.

4.8 Challenges

A major challenge this project faced and looked to address was the lack of coupled input power into the cavity on resonance. For a critically coupled Fabry-Perot optical cavity, nearly 100% of incident power should be transmitted through the cavity on resonance. Since all power is transmitted on resonance, no power is reflected from the cavity, leading to a dip in the observed reflection power.

This was not what was observed, however. Throughout the summer, the reflection dips were roughly 1% of incident power. This was also observed within the error signal, which also was roughly 1% of the expected strength. This issue propagated into difficulties in aquiring a lock, maintaining the lock, and measuring the finesse of the cavity. Due to these difficulities, a significant portion of the later stages of the project were spent addressing this limitation to progress towards obtaining a working setup for pulse locking.

The poor power coupling may be due to numerous factors, including damage to mirror coatings, excess intracavity losses due to dust, poor mode matching, unidentified noise sources, excess laser noise, and impedance matching issues. We decided that poor mode matching factor was the most likely culprit, as the setup should be equivalent to the previous working setup, outside of the mode matching solution and mirrors utilized. This does leave open the possibility that the new mirrors are damaged, or improperly cleaned. However, we decided to explore improving the mode matching, due to the inaccurate nature of beam profiling. This nature is evident, as small changes to the angle of the profiler, or specks of dust on the profiler lead to significant changes in the measured beam waist.

To improve the mode matching, we profiled the beam from laser output until the cavity, instead of only after the FI. We also ensured that the beam was centered on each optic, so that the profile propagated as expected.

To improve the accuracy of the new profile, we collected many more points for the profile. We also utilized a more accurate beam profiler, switching from the WinCamD to a scanning slit profiler. This is the case as the WinCamD has a much higher variance measurement to measurement than the scanning slit profiler, and it is much more susceptible to dust accumulation affecting measurements.

Below, Figure 11 shows an example of the updated beam profile, which will be utilized going forward to obtain a more accurate mode matching solution. It should also be noted that the fit from this update profile does deviate significantly from the fit derived from the prior profile. We expect this updated profile to be more accurate, as significant effort was spent ensuring the new profile was reproducible. We also utilized the scanning slit profiler, which had less variance measurment to measurement, making the profile more accurate.

Finally, it is important to acknowledge that it is possible that the narrow linewidth of the cavity ($\cong 250Hz$) is much smaller than the effective laser linewidth while locked. This would lead to only a small fraction of light coupling into the cavity even when the laser is locked to the cavity resonance. This possibility will be further explored once the new mode matching solution is implemented, and can be improved through utilizing the OLTF to inform improvements to the PDH lock.

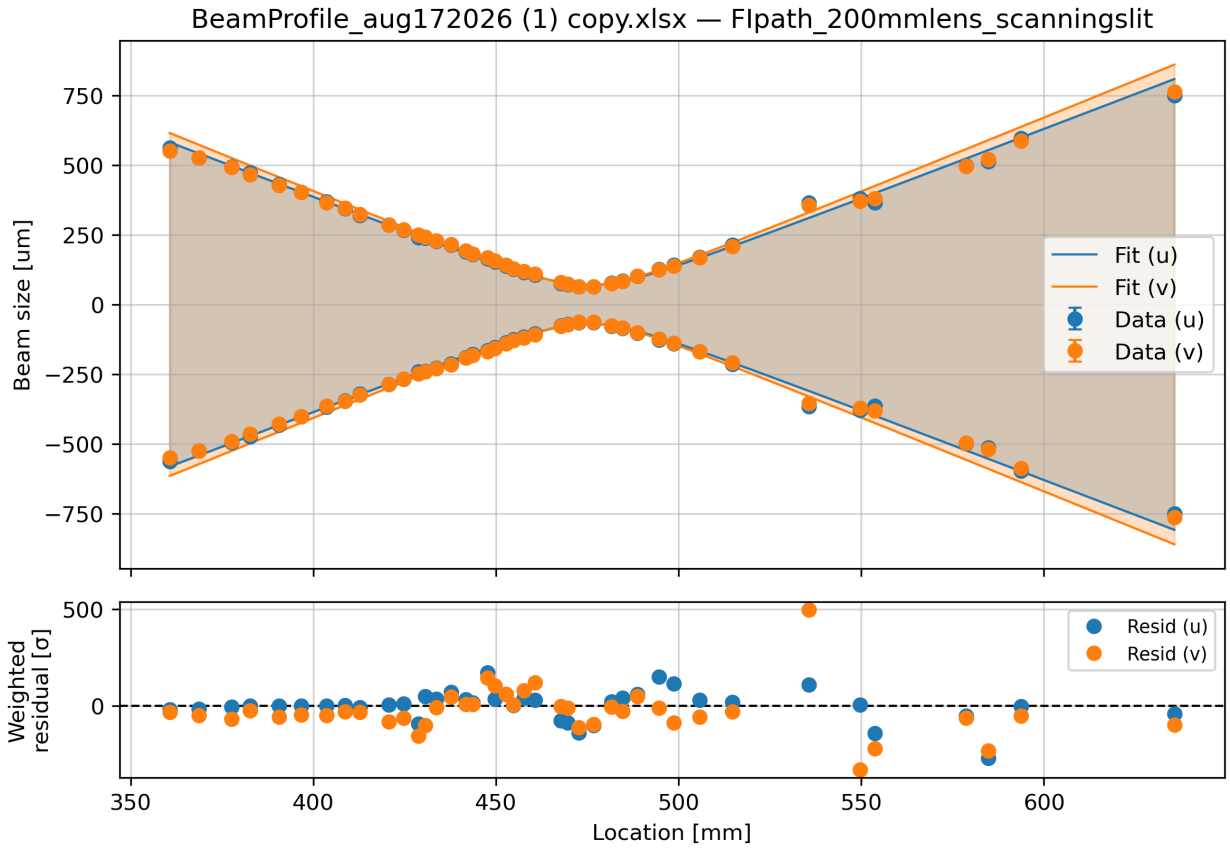


Figure 11: Update beam profile, with the Faraday isolator removed from the beam path.

5 Future Steps

Work throughout the summer has resulted in significant progress towards examining pulsed laser dynamics. Although we did not have enough time to explore pulsed laser operation this summer, this section will cover the immediate future steps for the project, including how we can lock the laser to the cavity under the pulsed regime.

5.1 Pulse Locking

To perform pulse locking, we require that the the pulse rate of the laser, f_{rep}, precisely matches the FSR of the cavity. This way, each incident pulse adds coherently with prior pulses that have a round trip time of $\tau_{circ} = \frac{1}{FSR} \simeq 7$ ns.

The mismatch between the repetition rate of the MZ-EOM and the cavity FSR can be defined as

$$\Delta f \equiv f_{rep} - \text{FSR}, \tag{16}$$

with the pulse stacking condition of $\Delta f = 0$.

5.2 Pulse Characterization

Prior to implementing a pulse lock, the strict pulse stacking condition will require the characterization of the pulses produced by the MZ-EOM. This includes the temporal shape and duration of the pulses, which we desire to be a square wave of 1 ns duration. This can be measured utilizing a fast PD and oscilloscope with bandwidths above 1 GHz to resolve the nanosecond pulses.

Once the characterization of the pulses is complete, and it has been ensured that the MZ-EOM can produce clean pulses at a steady repetition rate, the next step will be to implement the pulse lock.

5.3 Dither Lock

To ensure that f_{rep} stays equal to the FSR ($\Delta f = 0$), we will employ a dither lock. This is required because the transmitted power through the cavity is symmetric about resonance, so simply tracking the transmitted power provides no information on which way to correct the pulse frequency.

With a dither lock, the pulse rate is sinusoidally modulated at a frequency Ω, allowing for the recovery of direction information for feedback. The modulation is applied to the RF port of the MZ-EOM. Then, the mismatch between the dither frequency and cavity resonance is

$$\Delta f(t) = \Delta f + \Delta f_d \cos(\Omega t) \tag{17}$$

where Δf is offset we are trying to drive to zero, and Δf_d is the dither amplitude.

To obtain the error signal, we can examine the signal the transmission PD will observe.

Letting $V(\Delta f)$ be the voltage signal from the transmission PD and Taylor expanding expanding about the current operating point Δf for small modulation Δf_d, we get

$$V(t) = V(\Delta f) + \frac{dV}{d(\Delta f)}\,\Delta f_d \cos(\Omega t) + \frac{1}{2}\frac{d^2V}{d(\Delta f)^2}\,\Delta f_d^2 \cos^2(\Omega t) + \mathcal{O}(\Delta f_d^3). \tag{18}$$

Then, with small dither amplitude higher order terms can be dropped. To isolate the first-order term, a lock-in amplifier within the Moku can demodulate the voltage signal at frequency Ω and then pass through a low-pass filter. We can then see the zeroth order term will not survive the filter, but the first order term will contain a DC component due to the trig identity

$$2\cos^2(\Omega t) = 1 + \cos(2\Omega t), \tag{19}$$

and therefore survives the low-pass filter. With only the first-order term surviving, we have an error signal given by

$$\epsilon(\Delta f) \propto \left.\frac{dV}{d(\Delta f)}\right|_{\Delta f} \Delta f_d. \tag{20}$$

Finally, we can see more clearly how this provides an antisymmetric error signal by examining $V(\Delta f)$. Because $\Delta f = 0$ is a maximum, we can expand the transmitted signal about Δf,

$$V(\Delta f) \approx V_0 - A\,\Delta f^2, \tag{21}$$

where V_0 is the central voltage signal and

$$A \equiv -\frac{1}{2}\left.\frac{d^2V}{d(\Delta f)^2}\right|_{\Delta f=0} \tag{22}$$

is a constant capturing the curvature of the peak. Then, by differentiating we get

$$\frac{dV}{d(\Delta f)} = -2A\,\Delta f, \tag{23}$$

and substituting into the demodulated signal gives the error signal as

$$\epsilon(\Delta f) \propto \frac{dV}{d(\Delta f)}\,\Delta f_d = -2A\,\Delta f_d\,\Delta f. \tag{24}$$

Here we can see that the error signal vanishes when the repetition rate equals the FSR and is antisymmetric about resonance, allowing for feedback. In practice the transmission PD signal will be fed to the Moku, which performs the demodulation and applies a PID loop to the the signal applied to the MZ-EOM.

It is important to note the bandwidth limitations of this lock. Because the transmitted field responds to a change in Δf only on the timescale of the photon lifetime, the cavity acts as a low-pass filter on the error signal with a corner frequency at the cavity linewidth of approximately 200 Hz. Because of this low bandwidth, it will be necessary to determine the FSR of the cavity to high precision first to set the repetion rate of the pulses as close to this exact value as possible.

6 Conclusion

During this project, progress towards understanding the pulse dynamics in a demonstration optical enhancement cavity for the purpose of laser fusion was made. A key objective of this project was to establish a working Fabry-Perot optical enhancement cavity within a new vacuum setup. Progress was made towards this objective, with key results being achieving and analyzing a stable lock to the cavity with a CW laser. Solutions to a lack of coupled input power were also examined, and an improved characterization of the input beam profile were completed.

With this work, immediate next steps involve measuring the power coupling, measuring the cavity finesse and FSR, and characterizing the pulsed laser characteristics. Once this is complete, a pulse lock can be obtained by implementing a dither lock, where work will inform future BLF work on the larger scientific cavities.

References

[1] H. Abu-Shawareb *et al.* (Indirect Drive ICF Collaboration). *Achievement of target gain larger than unity in an inertial fusion experiment*. Phys. Rev. Lett., 132, 065102 (2024). https://journals.aps.org/prl/abstract/10.1103/PhysRevLett.132.065102

[2] C. Cahillane and G. Mansell. *Review of the Advanced LIGO gravitational wave observatories leading to observing run four*. Galaxies, 10, 36 (2022). https://arxiv.org/pdf/2202.00847

[3] A. Sunahara, G. Raj, T. Cohen, P. M. Pattison, P. Rudy, Y. Ohara, S. Iizuka, H. Ohta, and S. Nakamura. *Laser-based inertial fusion energy system enabled by optical enhancement cavities and a direct-drive configuration reactor*. Opt. Express, 33, 47104–47120 (2025). https://opg.optica.org/oe/fulltext.cfm?uri=oe-33-22-47104

[4] T. Cohen, J. Mance, S. Gandrothula, K. Arai, F. S. Carcoba, H. Ohta, P. M. Pattison, P. Rudy, N. Svadlenak, C. Smith, R. Fukuda, S. Iizuka, Y. Ohara, K. Tsubakimoto, R. Adhikari, and S. Nakamura. *Recent progress for commercializing IFE based on a novel high efficiency 10 MJ laser and high gain fuel target*. Proc. SPIE, 13358, 13358-4 (2025). https://bluelaserfusion.com/wp-content/uploads/2025/07/BlueLaserFusion-SPIE-2025_Manuscript.pdf

[5] C. Bond, D. Brown, K. A. Strain, and A. Freise. *Interferometer techniques for gravitational-wave detection*. Living Rev. Relativ., 19, 3 (2016). https://arxiv.org/abs/0909.3661

[6] E. D. Black. *An introduction to Pound–Drever–Hall laser frequency stabilization*. Am. J. Phys., 69, 79–87 (2001).https://www.agpohl.physik.uni-mainz.de/files/2023/06/AmJPhys69_79_2001_Black_Intro_PDH.pdf

[7] Wikipedia contributors. *Pound–Drever–Hall technique*. Wikipedia, The Free Encyclopedia. https://en.wikipedia.org/wiki/Pound%E2%80%93Drever%E2%80%93Hall_technique.

[8] M. Weichman. *Simulating Cavity Transmission Spectra* (2023). https://weichman.princeton.edu/wp-content/uploads/2023/08/cavity_transmission_spectra.pdf

[9] P. H. Roberts. *Pound–Drever–Hall Laser Frequency Stabilization*. California Institute of Technology. http://pmaweb.caltech.edu/~ph77/labs/optics/pdh.pdf

[10] N. Ismail, C. C. Kores, D. Geskus, and M. Pollnau. *Fabry–Pérot resonator: Spectral line shapes, generic and related Airy distributions, linewidths, finesses, and performance at low or frequency-dependent reflectivity*. Opt. Express, 24, 16366–16389 (2016). https://opg.optica.org/oe/abstract.cfm?URI=oe-24-15-16366

7 Acknowledgements

I would like to thank the NSF for sponsoring this research project. I would also like to thank Professor Adhikari and Dr. Bolingbroke for their help and mentorship throughout this project.